Millimetre-Wave Dual-Polarized Differentially-Fed 2D Multibeam Patch Antenna Array

Qingling Yang, Steven Gao, *Fellow, IEEE*, Qi Luo, *Senior Member, IEEE*, Lehu Wen, Yong-Ling Ban, Xiaofei Ren, Jian Wu, Xuexia Yang, *Senior Member, IEEE*, and Ying Liu, *Senior Member, IEEE*

***Abstract*—In this paper, a novel millimetre-wave dual-polarized 2D multibeam antenna array incorporating differentially-fed antenna elements is proposed to achieve high cross-polarization discrimination (XPD) when the beams scan to the maximal pointing angles. The antenna element is composed of a SIW cavity with four shorted patches placed inside, and it is differentially excited for dual-polarization by a pair of feeding strips and transverse slots beneath the patches. Differential excitation is realized by a power divider designed on two laminate layers. Two Butler Matrices placed perpendicularly with each other in different laminates are employed to generate four tilted beams with dual-polarization. A 2×2 dual-polarized 2D multibeam antenna array working at 28 GHz is designed, fabricated, and measured. The operation bandwidth of the antenna is 26.8 GHz – 29.2 GHz. The improvement in the XPD is experimentally demonstrated by far-field measurement. When the beams scan to 30° off the boresight, the measured XPDs are 28 dB at the centre frequency and higher than 25 dB over the operation bandwidth, which confirms that the cross-polarized radiation in the 2D multibeam antenna array is suppressed by using the differential-feeding technique. The measured gain is in the range from 7.6 dBi to 10.5 dBi.**

***Index Terms*—Butler Matrix, cross-polarization, differential feeding, dual-polarization, millimetre-wave, multibeam antenna, patch antenna**

I. Introduction

WIRELSS communications have experienced considerable growth in the past decade due to ever-increasing handheld devices accessing to real time data. For 5G millimetre-wave (mmWave) applications, the multibeam antenna array able to steer beams in two dimensions and operate with dual-polarization is an attractive candidate to achieve multispot coverage and high channel capacity [1] – [7]. The dual-polarized antenna array is usually required to have high cross-polarization discrimination (XPD) and high isolation between ports for different polarizations so as to improve the signal-to-noise ratio and reduce the channel interference. However, it is difficult to achieve good XPD in 2D multibeam antenna arrays, because high cross-polarized radiation occurs when beams scan off the boresight. In addition, the intricate beamforming networks and high integration complexity also impose challenges on designing a dual-polarized 2D multibeam antenna array.

A number of techniques to realize beamforming networks for 2D multibeam antenna arrays have been reported. Multibeam antennas realized using dielectric lenses and reflectors are simple, but they are bulky and expensive [8], [9]. To reduce the cost and size, the antenna arrays driven by Butler Matrices or Rotman Lenses are more preferable in many scenarios since they can be realized with planar laminates. To generate multiple beams in two dimensions, the beamforming networks composed of cross-connected Butler Matrices or Rotman Lenses are considered in some designs [10] – [12]. However, these designs have low integration, high loss and high cost. In general, to design a mmWave multibeam antenna array, the slot and traditional patch antennas are frequently selected as the radiating element thanks to their simple structure and ease of integration [13] – [20]. As reported in [15], low side-lobe levels (SLLs) are obtained in the multibeam slot antenna array by tapering the amplitude distribution at the array ports of the beamforming network. The antenna element in [20] is realized by placing a parasitic patch over a square SIW cavity to achieve wide bandwidth. Another antenna type widely used in mmWave multibeam antenna arrays is magneto-electric (ME) dipoles due to their wide bandwidth, broad beamwidth and symmetric radiation patterns [21] – [24]. As seen from these designs, most of the antennas are only able to steer beams in one dimension and operate with a single polarization. Particularly, cross-polarized radiation in these multibeam antenna arrays is not well suppressed, resulting in low XPDs which is less than 15 dB when beams scan off the boresight. Although the multibeam antenna array proposed in [24] is able to steer beams in two dimensions and operate with dual-polarization, its XPDs are degraded to 10 dB when the beams are at the maximal pointing angles.

In this paper, we introduce a novel dual-polarized 2D multibeam antenna array incorporating differential-fed antenna elements. The differential feeding technique has been widely used in modern antenna designs [25] – [26] in order to achieve high port isolation, high XPD and symmetric radiation patterns. In our design, the antenna element is composed of a SIW cavity with four shorted patches placed inside, and it is differentially excited for dual-polarization by a pair of feeding strips and

This work was funded by China Research Institute of Radiowave Propagation, Engineering and Physical Sciences Research Council (EPSRC) under grants EP/P015840/1, EP/N032497/1 and EP/S005625/1. (*Corresponding author: Qingling Yang*)

Q. Yang, S. Gao, Q. Luo and L. Wen are with the School of Engineering and Digital Arts, University of Kent, Canterbury CT2 7NZ, UK.

Y. Ban is with the School of Electronic Science and Engineering, University of Electronic Science and Technology of China, Chengdu 611731, China.

X. Ren and J. Wu are with the China Research Institute of Radiowave Propagation, Xinxiang, Henan 453003, China.

X. Yang is with the School of Communication and Information Engineering, Shanghai University, Shanghai 200444, China.

Y. Liu is with the National Laboratory of Science and Technology on Antennas and Microwaves, Collaborative Innovation Centre of Information Sensing and Understanding, Xidian University, Xi'an 710071, Shaanxi, China. liuying@mail.xidian.edu.cn

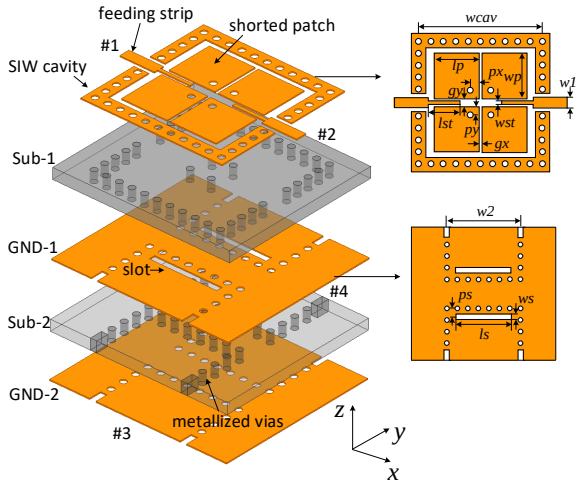

Fig. 1. Configuration of the proposed differentially-fed dual-polarized antenna. (Dimensions: $w_{cav} = 6.4$ mm, $l_p = 2.2$mm, $w_p = 2.2$mm, $g_x = 0.15$ mm, $g_y = 0.4$ mm, $p_x = 0.425$ mm, $p_y = 0.4$ mm, $l_{st} = 1.55$ mm, $w_{st} = 0.15$ mm, and $w_1 = 0.5$ mm, $w_2 = 4.3$ mm, $l_s = 3.2$ mm, $w_s = 0.3$ mm, and $p_s = 0.5$ mm)

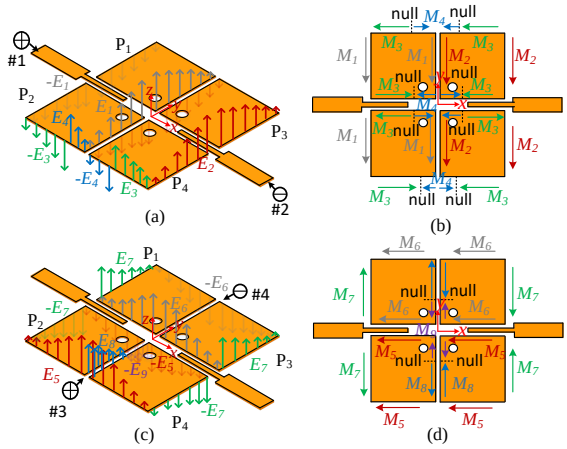

Fig. 2. (a) Electric field distribution, and (b) Equivalent magnetic current when differential port d1 is excited. (c) Electric field distribution, and (d) Equivalent magnetic current when differential port d2 is excited.

transverse slots beneath the patches. Differential excitation is realized by a power divider designed on two laminate layers. Two Butler Matrices placed perpendicularly with each other in different laminates are employed to generate four tilted beams with dual-polarization. A dual-polarized 2×2 2D multibeam antenna array working at 28 GHz is designed, fabricated and measured. It is demonstrated that the proposed design has the advantages of high XPD and simple configuration. When the beams scan to 30° off the boresight, the measured XPDs are 28 dB at the centre frequency and higher than 25 dB over the operation bandwidth. The measured results confirm that the cross-polarized radiation in the 2D multibeam antenna array is suppressed by using the differential-feeding technique.

This paper is organized as follows. Section II presents the configuration, the operation mechanism and design of the dual-polarized differentially-fed antenna element. In Section III, the feeding network designs including the Butler Matrix, the differential power divider and the interconnection structure are presented. Section IV shows the measured results of the multibeam antenna array. Section V concludes the paper.

II. Dual-Polarized Antenna

A. Antenna Configuration

The configuration of the proposed dual-polarized antenna is illustrated in Fig. 1, which is composed of a square SIW cavity and four patches. The SIW cavity is used to prevent potential surface-waves from propagating when beams steer off the boresight. Four inductive vias with a diameter of 0.3 mm and an offset position of (p_x, p_y) are used to connect the patches to the ground plane. The antenna is differentially excited for dual-polarization by different feeding structures. The feeding structure for exciting HP radiation is realized with a stepped microstrip line, which is small enough to be fitted between the patches. The feeding structure for exciting VP radiation is realized with SIWs in Sub-2. The SIW width is set to $w_2 = 4.3$ mm for avoiding higher order modes within the operation frequency of interest. To couple the input energy from the SIWs so as to excite the shorted patches in Sub-1, two transverse slots are etched on the top copper layer of Sub-2. According to the mixed-mode theory, the *S*-parameters of a differentially-fed antenna can be obtained from the single-ended four-port *S*-parameters [27]. Thus, to facilitate the analysis, port #1 and #2 are defined as the differential feeding port d1 for exciting HP radiation, and port #3 and #4 are defined as the differential feeding port d2 for exciting VP radiation. In this design, Sub-1 and Sub-2 are the Rogers 4003C laminates with a thickness of 0.508 mm, relative permittivity of 3.55, and the loss tangent of 0.0027. All the simulations in this work are performed by using the high frequency full-wave electromagnetic solver, ANSYS Electronics Desktop HFSS.

B. Working Mechanism

Similar to the traditional patch antennas, an intuitive way of analysing the working mechanism from the proposed antenna is based on the cavity-mode theory [28]. Fig. 2 shows the electric distribution and equivalent magnetic currents of the proposed differentially-fed dual-polarized antenna. To facilitate the analysis, the antenna is viewed as an array of four shorted patches P_1, P_2, P_3 and P_4. When signals input from the differential port d1, the shorted patches is excited for HP radiation by coupling from the feeding strips. It is seen from Fig. 2(a) that the electric fields radiated from each patch are identical. In addition, the electric field pattern from P_1 and P_2 (or P_3 and P_4) is quite similar to that of a traditional patch antenna resonating at TM_{010} mode. Thus, the antenna can be regarded as two patch antennas with the resonating length w_p and the width $(2l_p + g_y)$. As shown in Fig. 2(b), the magnetic currents M_1 and M_2 from the edges along the *y*-axis are in the same direction, indicating that constructive far fields are obtained in the *E*-plane (*xoz*-plane, $\phi = 0°$). The presence of the shorting vias helps to improve the impedance matching. However, it also makes the nulls between the magnetic currents M_3 and M_4 shift off the centre of each edge. The cross polarization in the *E*-plane caused by these *x*-directed magnetic

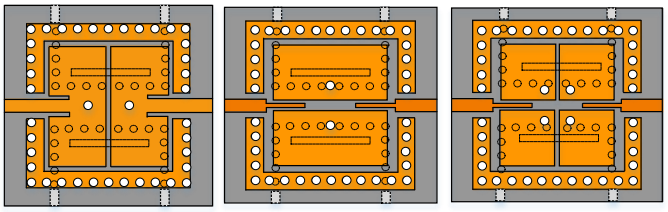

Fig. 3. Design process of the proposed differentially-fed dual-polarized antenna. (a) Ant-1. (b) Ant-2. (c) Proposed antenna.

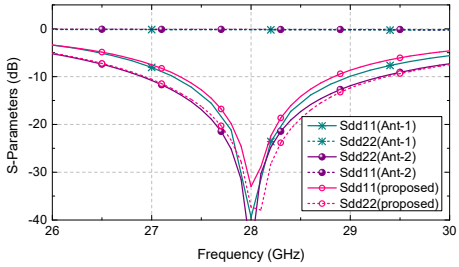

Fig. 4. Simulated results of the antennas in the design process.

currents would be very low because these currents are anti-symmetric along the x-axis. Similar observations can be found for the H-plane (yoz-plane, $\phi = 90°$). Thus, when differential port d1 is excited, the edges along the y-axis contribute to the effective field radiation, while the edges parallel to the x-axis constitute the non-radiating edges of the antenna.

When operating with VP, the antenna is excited by couplings from the transverse slots underneath the shorted patches. As the dominant mode of the feeding SIWs in Sub-2 is TE_{10} mode, the electric fields near the shorted-end wall of the feeding SIWs are vertically polarized, which results in longitudinal electric fields across the transverse slots. Therefore, the shorted patches placed above the transverse slots can be excited subsequently. In this case, the radiating edges are those parallel to the x-axis. As shown in Fig. 2(c), the electric fields from these edges are same as those from the radiating edges of a traditional patch antenna. In this case, the antenna can be considered as two patch antennas with the resonating length l_p and the width $(2w_p + g_x)$. Fig. 2(d) shows the magnetic currents when the antenna operates with VP. Constructive far fields are obtained in the E-plane (yoz-plane, $\phi = 90°$) as the magnetic currents M_5 and M_6 are in the same direction. The magnetic currents M_7, M_8 and M_9 from the edges along the y-axis are slightly different from those of Fig. 2(b). In this case, no magnetic current nulls are found at the external edges, while each internal edge has a null between the magnetic currents M_8 and M_9. In spite of this, the cross polarization caused by the y-directed magnetic currents would be also very small as these currents are anti-symmetric along the y-axis. Thanks to the differential feeding applied, the currents on the feeding strips are very weak when differential port d2 is excited, which ensures high isolation between the differential port d1 and d2.

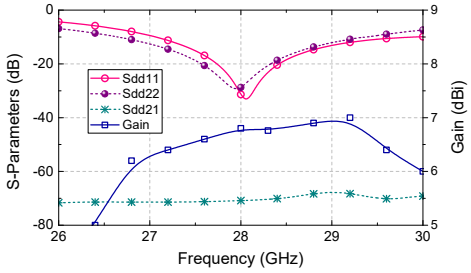

Fig. 5. Simulated S-parameters and gain of the proposed antenna.

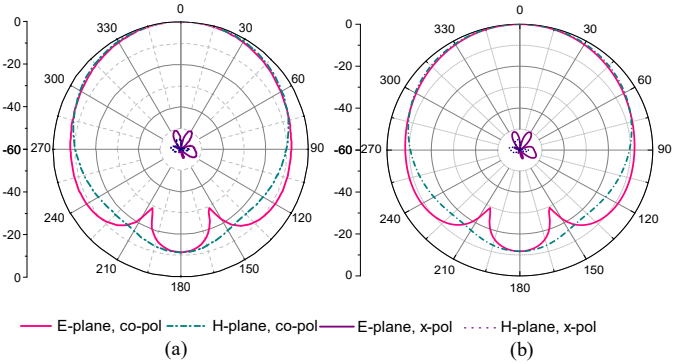

Fig. 6. Simulated radiation patterns of the proposed antenna at 28 GHz. (a) Differential port d1 is excited (HP). (b) Differential port d2 is excited (VP).

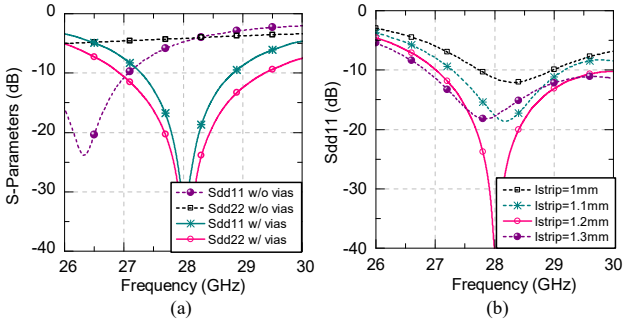

Fig. 7. (a) Simulated S-parameters with or without the shorting vias. (b) Simulated S_{dd11} by varying the length of the feeding strip.

C. Antenna Optimization

Due to constrained space and high design complexity, it is usually difficult to design a mmWave antenna array incorporating differentially fed antenna elements. To better illustrate the design process of the developed antenna, the reference antennas (Ant-1 and Ant-2) are shown in Fig. 3. As shown in Fig. 3(a), Ant-1 is realized with two patch antennas placed inside the SIW cavity, and the differential feeding pairs are perpendicularly placed for dual-polarization. The antenna can be considered as an inset-fed patch antenna when operating with HP. To improve the impedance matching, two inductive vias are placed beside the centre line. The length of the patch l_p decides the resonance frequency, and the width of the patch w_p affects the input impedance. The preliminary simulation shows that to achieve good impedance matching the patch length should be 0.9λ. However, it makes the patch non-

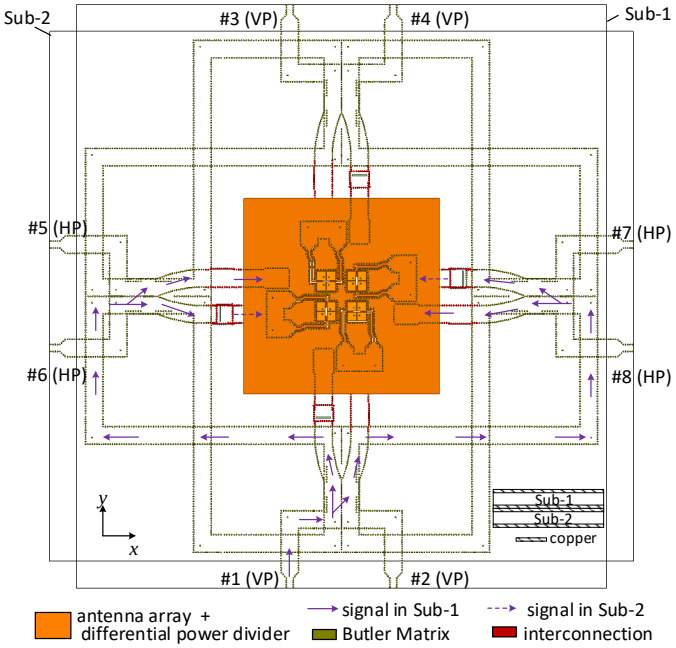

Fig. 8. Configuration of the proposed dual-polarized 2D multibeam array antenna.

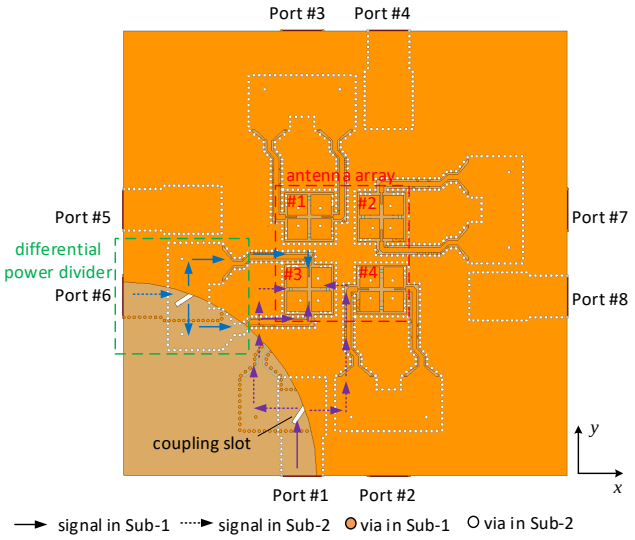

Fig. 9. Layout of the 2×2 antenna array and the differential power dividers.

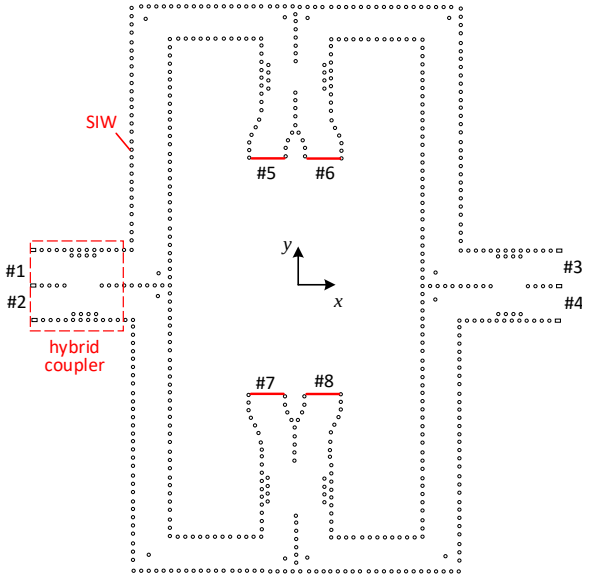

Fig. 10. Layout of the designed Butler Matrix.

resonant when the antenna operates with VP. As can be seen from Fig. 4, signals input from the differential port d2 are totally reflected. To investigate the resonance characteristics of the proposed antenna when operating with VP, Ant-2 is developed by placing the patches above the coupling slots. The feeding strips for exciting HP radiation is located between the two patches. The antenna can be considered as a slot-coupled patch antenna when operating with VP. The simulated results presented in Fig. 4 show that good impedance matching is achieved at differential port d2. However, in this case, strong reflection is observed at the differential port d1. To realize good impedance matching at both differential ports, the proposed antenna is designed by splitting the patch into four elements. The proposed antenna can be taken as a combination of Ant-1 and Ant-2. The dimension of each patch element is 2.6 mm $\times$2.6 mm ($\approx 0.39\lambda \times 0.39\lambda$), which enables the antenna to resonate when it is excited at the differential port d1 or d2. As shown in Fig. 4, the splitting of the patch has no influence on the performance of this differentially fed antenna. Thus, the proposed antenna is an inset-fed patch antenna when it operates with HP, and a slot-coupled patch antenna when it operates with VP.

Fig. 5 shows the simulated performance of the proposed antenna. The overlapped impedance bandwidth for S_{dd11} and S_{dd22} less than –10 dB is 8.6%, from 26.8 GHz to 29.2 GHz. The antenna exhibits high port isolation, which is higher than 68 dB. Stable gain is achieved over the operation bandwidth, which is in the range of 6.2 dBi–7 dBi. The simulated radiation patterns in E-plane and H-plane are shown in Fig. 6. It is observed from Fig. 6(a) that the proposed antenna has symmetrical radiation patterns in the E-plane and the H-plane when the differential port d1 is excited. The –3 dB beamwidth of the radiation patterns is 86° in both planes, and the XPD is higher than 46 dB within the beamwidth. As shown in Fig. 6(b), similar radiation patterns are also obtained when the differential port d2 is excited.

The shorting via connecting the patch elements to the ground plane help to improve the impedance matching of the proposed antenna. As shown in Fig. 7(a), the performance of S_{dd11} and S_{dd22} is very sensitive to the introduced vias. The resonant frequency increases with the presence of the shorting vias when differential port d1 is excited. Without introducing the shorting vias, no resonance is observed over the bandwidth when differential port d2 is excited. In addition, the impedance matching at differential port d1 is also affected by the feeding strip length l_{strip}. As shown in Fig. 7, the resonance shifts to the lower frequency with the increase of strip length, because the inset feeding leads to longer electric

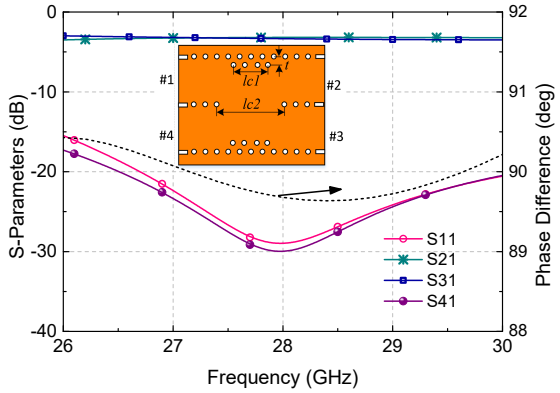

Fig. 11. Layout and S-parameters of the designed hybrid coupler. (Dimensions: l_{c1}=3.7mm, t=0.65mm, l_{c2}=5.4mm)

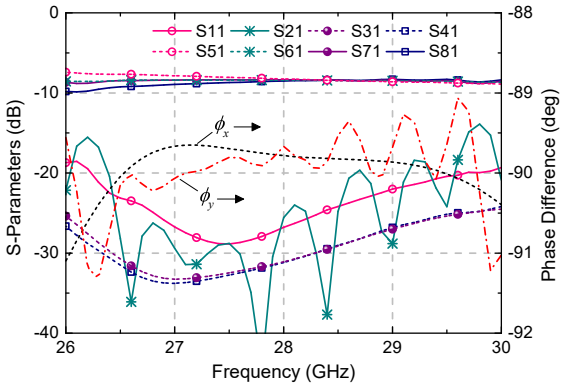

Fig. 12. Simulated performance of the designed Butler Matrix.

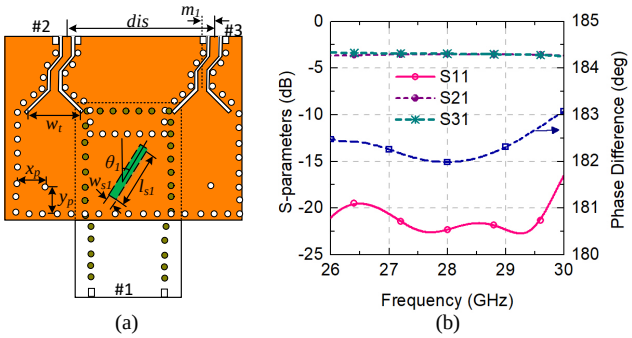

Fig. 13. Differential power divider. (a) Layout (w_t = 3.6 mm, x_p = 1.66 mm, y_p = 1.46 mm, l_{s1} = 3.17 mm, w_{s1} =0.3 mm, $\theta_1 = 33.56°$, m_1 = 0.7 mm, dis = 6.8 mm). (b) Simulated performance.

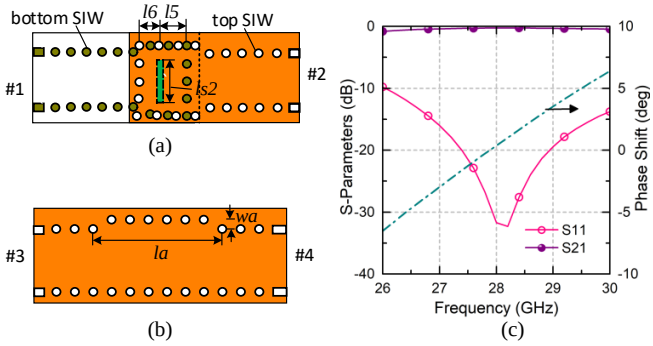

Fig. 14. (a) Interconnection (l_5 = 3 mm, l_6 = 0.89 mm, l_{s2} = 3.63 mm). (b) Reference SIW (l_a = 6.27 mm, w_a = 0.2 mm). (c) Simulated results.

current path for the patch antenna. When the strip length l_{strip} increases to 1.2 mm, the resonance frequency shifts to 28 GHz with $S_{dd11} < -30$ dB. The presence of feed strips almost has no effect on S_{dd22} due to high isolation between the differential port d1 and d2.

III. Multibeam Antenna Array

A. Configuration of the Multibeam Antenna Array

Fig. 8 shows the configuration of proposed dual-polarized 2D multibeam antenna array. It consists of 2×2 antenna elements, two SIW Butler Matrices, eight differential power dividers, and four interconnection structures. The two Butler Matrices are placed perpendicularly to each other in different layers so as to generate four tilted beams with dual-polarization. The vertical Butler Matrix connected to port #1–#4 is used to excite VP beams, and the horizontal Butler Matrix connected to port #5–#8 is used to excite HP beams. The Butler Matrices for HP and VP are designed in the bottom laminate (Sub-2) and the top laminate (Sub-1), respectively. The differential power divider is used to differentially excite the antenna elements. In order to avoid intersection, an interconnection structure is located between the Butler Matrix and the differential power divider. The signal paths when port #1 is excited are also shown in Fig. 8. The signals traveling in Sub-1 is denoted by the solid arrows and the signals in Sub-2 is denoted by the dotted arrows. To better illustrate the path of signals from the power divider to each antenna element, the detailed layouts of the differential power divider and the 2×2 antenna array are illustrated in Fig. 9. The differential power divider is designed in two laminate layers, and interlayer signal transmission is achieved by a coupling slot etched on the ground plane. Because the feeding port of the antenna element for exciting VP is located in Sub-2, the differential power divider connected with port #1 is anti-symmetric with the one that is connected with port #2. The antenna element spacing in x- and y- direction is chosen as 7.5 mm ($0.7\lambda_0$).

B. Butler Matrix

Fig. 10 presents the structure of the designed Butler Matrix, which consists of four hybrid couplers. No additional phase shifters are needed in this Butler Matrix structure. Ideally, fixed phase differences ($\pm 90°$, $\pm 90°$) can be obtained between the output ports in x- and y-direction. For details, Table. I gives the theoretical phase responses at port #5 – #6 when port #1 – #4 is excited, respectively. A hybrid coupler can be considered as an equal power divider having 90° phase difference between the direct port and coupling port [29]. Fig. 11 shows the layout and the simulated results of the designed hybrid coupler. The simulated operation bandwidth for $S_{11} < -15$ dB is from 26 GHz to 30 GHz. The transmission coefficients from port #1 to port #2 and #3 are in the range of 3.2 ± 0.4 dB, and the

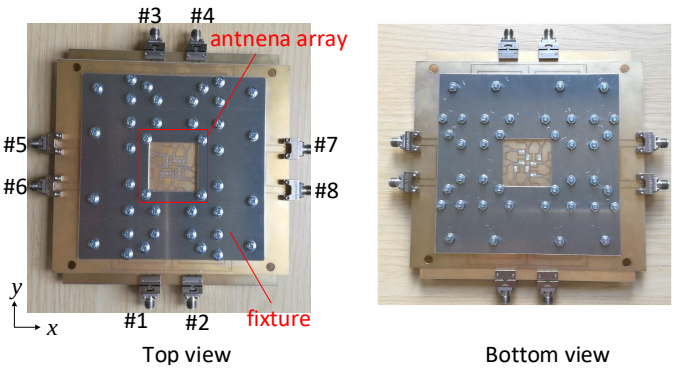

Fig. 15. Top and bottom view of the fabricated array antenna.

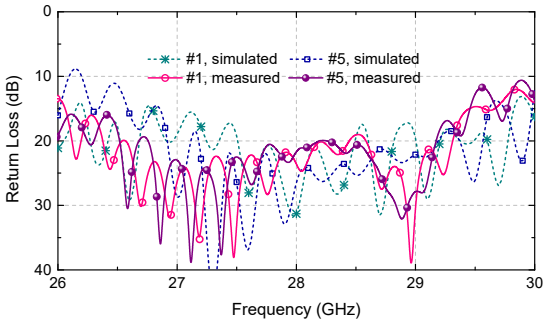

Fig. 16. Measured and simulated return loss for port #1 and #5.

TABLE I
THEORETICAL OUTPUT PHASE DIFFERENCES OF THE BUTLER MATRIX

#1		ϕ_x	ϕ_y
0° (#5)	−90° (#6)	−90°	90°
−90° (#7)	180° (#8)		
#2		ϕ_x	ϕ_y
−90° (#5)	180° (#6)	−90°	−90°
0° (#7)	−90° (#8)		
#3		ϕ_x	ϕ_y
−90° (#5)	0° (#6)	90°	90°
180° (#7)	−90° (#8)		
#4		ϕ_x	ϕ_y
180° (#5)	−90° (#6)	90°	−90°
−90° (#7)	0° (#8)		

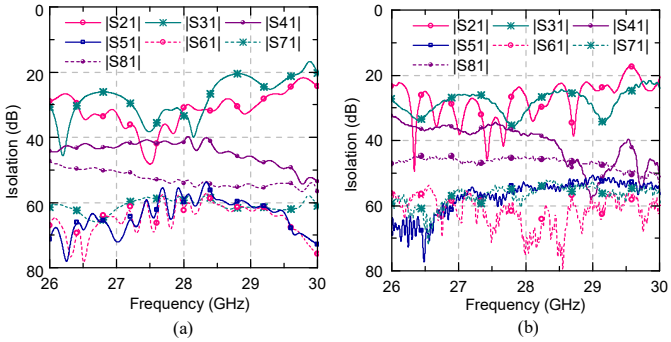

Fig. 17. Isolations between port #1 and port #2 to #8. (a) Simulated. (b) Measured.

obtained phase difference of signals output from port #2 and #3 is $90 \pm 0.5^\circ$ over the bandwidth. Port #4 is well isolated from port #1 within the bandwidth.

Fig. 12 shows the simulated results of the designed Butler Matrix. The impedance bandwidth for $S_{11} < -20$ dB is wider than 14% (from 26.3 GHz–29.8 GHz). Besides, the isolation between any two input ports is higher than 15 dB over the bandwidth. The insertion loss of this Butler Matrix is less than 1.6 dB from 26.8 GHz to 29.2 GHz. Simulated phase responses of the designed Butler Matrix are also included in Fig. 12. The phase differences between the output ports are in the range of $-90 \pm 1^\circ$ from 26 GHz to 30 GHz, which are very close to the theoretical values.

C. Differential Power Divider

Fig. 13(a) shows the layout of the designed differential power divider. Port #1 is the input port, and port #2 and #3 are the output ports. The differential power divider can be taken as an equal power divider that enables the signals out from port #2 and #3 to be out-of-phase. In this design, the structure of the power divider is realized by using two laminate layers. Interlayer signal transmission is achieved by etching a coupling slot on the ground plane. To improve the impedance matching at port #1, the slot is slanted with an angle of θ_1. The meandered three-stage grounded co-planar waveguides, which is $m_1 = 0.7$ mm away from the centre line, are used to avoid overlapping between two neighbouring differential power dividers. Fig. 13(b) shows the simulated results of the designed differential power divider. The impedance bandwidth for S_{11} <–20 dB is from 26 GHz to 29.7 GHz. The received power at port #2 and #3 is -3.3 ± 0.15 dB lower than the input power at port #1 over the bandwidth. The phase difference between the two output ports is in the range of $182.5^\circ \pm 0.5^\circ$ over the bandwidth, which indicates that differential excitation to the antenna element is achieved.

D. Interconnection

To make the feeding networks for different polarizations separated in different layers without intersection, an interconnection structure is designed, as shown in Fig.14(a). The interconnection consists of two SIWs situated in different layers. To realize interlayer transmission, a transverse slot is etched at the common ground plane of the two SIWs. High coupling efficiency can be obtained by tuning the lengths l_5 and l_6. As shown in Fig. 14(b), an equal-length unequal-width reference SIW is designed to compensate the additional phase introduced by the interconnection. The desired 0° phase shift between the interconnection and the reference SIW can be obtained by varying the length l_a and width w_a. Fig. 14(c) shows the simulated S-parameters of the interconnection and its phase shift relative to the reference SIW. The operation bandwidth for $S_{11} < -10$ dB is 14.3% (from 26 GHz–30 GHz). Within this bandwidth, the insertion loss is from –0.52 dB to –0.28 dB. The phase difference with a deviation of $0.2 \pm 6.6^\circ$ is achieved over the operation bandwidth.

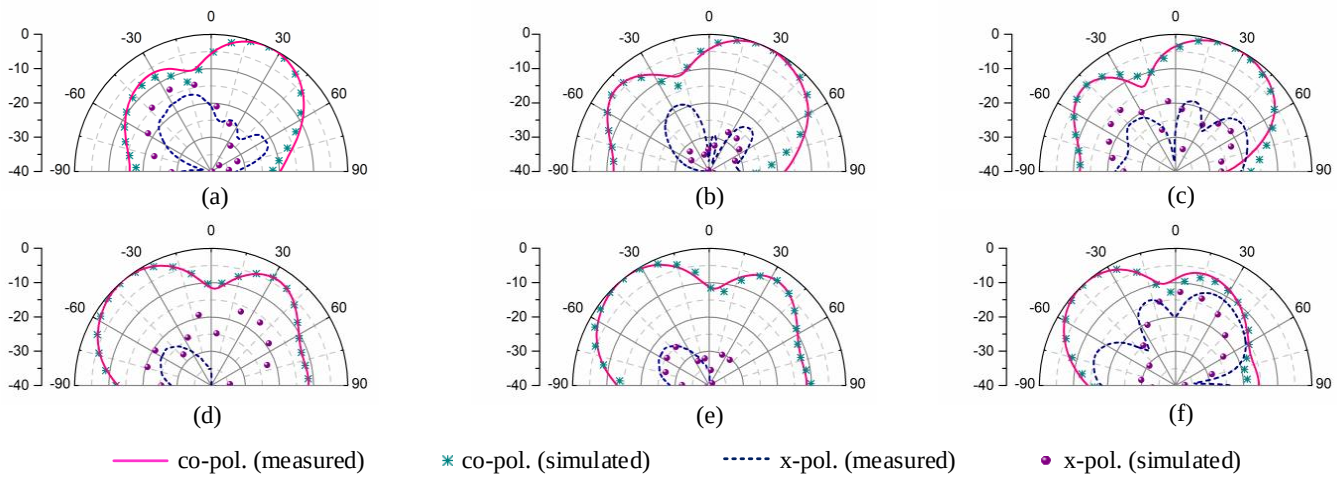

Fig. 18. Simulated and measured radiation patterns of the proposed multibeam array antenna with VP when port 1 is excited. (a)26.8 GHz @ quasi *E*-plane. (b) 28 GHz @ quasi-*E*-plane. (c) 29.2 GHz @ quasi-*E*-plane. (d)26.8 GHz@ quasi-*H*-plane. (e)28 GHz @ quasi-*H*-plane. (f) 29.2 GHz @ quasi-*H*-plane.

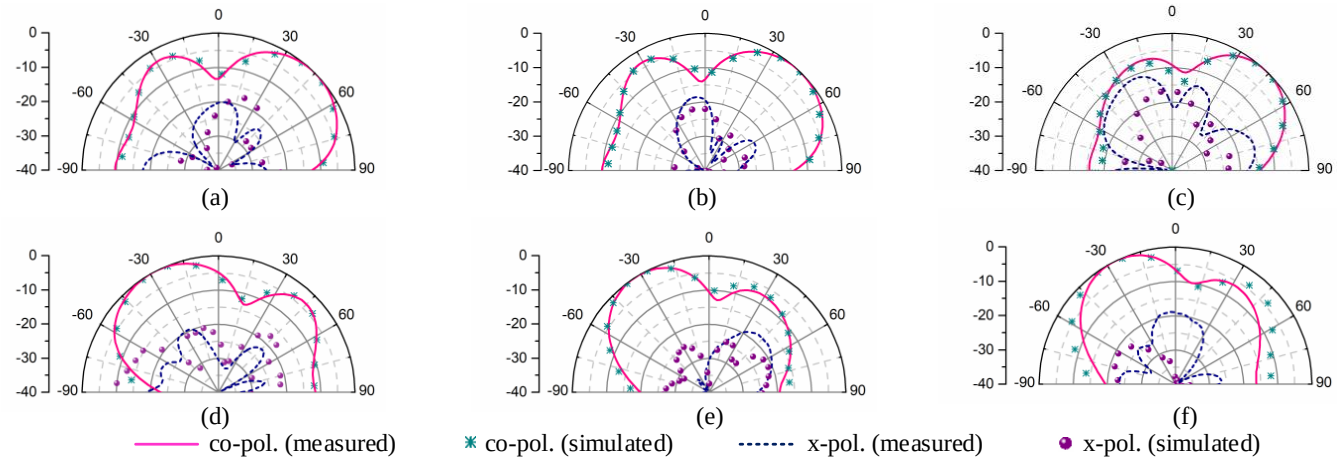

Fig. 19. Simulated and measured radiation patterns of the proposed multibeam array antenna with HP when port 5 is excited. (a)26.8 GHz @ quasi-*E*-plane. (b) 28 GHz@ quasi-*E*-plane. (c) 29.2 GHz @ quasi-*E*-plane. (d)26.8 GHz @ quasi-*H*-plane. (e)28 GHz @ quasi-*H*-plane. (f) 29.2 GHz @ quasi-*H*-plane.

IV. Measured Results

A. Return Loss and Port Isolation

The fabricated prototype of the proposed multibeam antenna array is given in Fig. 15. The laminate layers are tightly pressed by two aluminium fixtures to ensure good interlayer transmission. The network analyzer Anritsu 37397C is used to perform the *S*-parameters measurement. Fig. 16 presents the simulated and measured return losses ($|S_{11}$ and $|S_{55}|$) at port # 1 and #5, which are in good agreement. The measured impedance bandwidth for return loss higher than 10 dB is 14.3%, from 26 GHz to 30 GHz. Due to the presence of the feeding networks, the measured and simulated bandwidths of the multibeam antenna array are slightly wider than the bandwidth of the antenna element.

The measured and simulated isolations between port #1 and port #2 – #8 are presented in Fig. 17. It can be seen that the measured and simulated results are in good agreement. High port isolations are achieved in this antenna array. The measured isolations between the ports for exciting radiated waves with the same polarization, $|S_{21}|$ to $|S_{41}|$, are higher than 21 dB over the operation bandwidth 26.8 GHz–29.2 GHz. The measured isolations between the ports for exciting the radiated waves with different polarization, $|S_{51}|$ to $|S_{81}|$, are higher than 46 dB over the bandwidth. Due to the symmetrical structure of the proposed multibeam array antenna, the performance of other ports is similar to the above results.

B. Radiation Patterns and XPD

The theoretical beam pointing angles for 2D beam scanning antenna arrays in the spherical coordinate are given by

$$\theta_p = \text{asin}\sqrt{\left(\frac{\phi_x}{kd_x}\right)^2 + \left(\frac{\phi_y}{kd_y}\right)^2}, \phi_p = \text{atan}\left(\frac{\phi_x d_x}{\phi_x d_y}\right) \quad (1)$$

where ϕ_x and ϕ_y are the fixed phase differences in *x*- and *y*-direction which are listed in Table. I. d_x and d_y are the element spacing in *x*- and *y*- direction, and they are 7.5 mm ($\approx 0.7\lambda_0$) in this design. *k* is the wavenumber in free space. The designed multibeam antenna array generates four 2D radiation patterns for HP or VP polarization corresponding to four input ports. The calculated maximal beam pointing angles are (30°, 45°),

TABLE II
COMPARISON BETWEEN THE DESIGNED MULTIBEAM ARRAY ANTENNA AND THE REPORTED WORKS

Ref.	Ant. Type	Pol.	XPD	BW	h/λ	Used Sub.	Ant. Elements	Element Spacing	SLL	Gain
[15]	slot	single	10 dB	3.6%	0.07	3	4×4	n.a.	–13 dB	13.8 dBi
[19]	patch	single	10 dB	16.7%	n.a.	2	2×4	$0.5\lambda_0\times0.6\lambda_0$	–5 dB	11.6 dBi
[20]	cavity-backed patch	single	15 dB	36.2%	0.25	4	2×2	$0.6\lambda_0\times0.6\lambda_0$	–4 dB	11 dBi
[23]	ME-dipole	single	12 dB	16.4%	0.23	4	4×4	$0.57\lambda_0\times0.57\lambda_0$	–6 dB	14.7 dBi
[24]	ME-dipole	dual	10 dB	22%	0.21	3	2×2	$0.6\lambda_0\times0.6\lambda_0$	–7 dB	12 dBi
This work	differentially-fed cavity-backed shorted patch	dual	28 dB	8.6%	0.09	2	2×2	$0.7\lambda_0\times0.7\lambda_0$	–4 dB	10.5 dBi

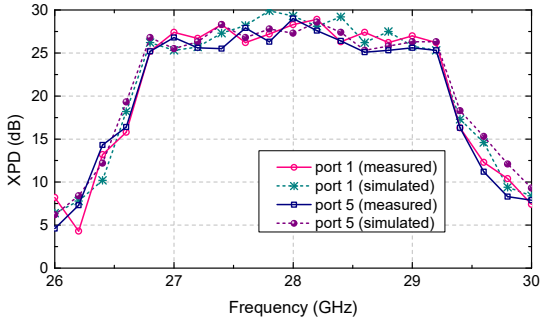

Fig. 20. Minimum XPDs at different frequencies when port #1 and #5 is excited.

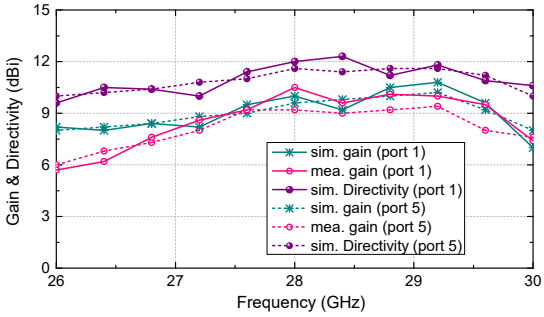

Fig. 21. Simulated gain, directivity and measured gain when port #1 and port #5 is excited, respectively.

(30°, 135°), (30°, 225°) and (30°, 315°) in the spherical coordinate when port #1 – #4 is excited, respectively. By using the definitions of quasi-E-plane and quasi-H-plane presented in [30], the measured and simulated radiation patterns of the fabricated multibeam antenna array at 26.8 GHz, 28 GHz and 29.2 GHz are obtained. Fig. 18 shows the radiation patterns when port #1 is excited for VP, and Fig. 19 shows the radiation pattern when port #5 is excited for HP. The measured results are in reasonable agreement with the simulations. It is seen that the radiation patterns are stable at different frequencies when the beams scan to the maximal pointing angles, and the radiation patterns with different polarizations are very similar to each other. At 28 GHz, the measured beam pointing angle is $(28°, 41°)$ when port #1 is excited, and the measured beam pointing angle is $(34°, -43°)$ when port #5 is excited. The measured pointing angles are slightly different from the theoretical ones $(\pm30°, \pm45°)$ due to fabrication tolerance and the presence of the large ground plane introduced by the feeding network.

Fig. 20 shows the minimum XPDs of the designed multibeam array antenna at different frequencies. High XPDs are achieved in the fabricated antenna array when the beams scan to the maximal pointing angles. Within the operation frequency band, the XPDs are higher than 25 dB. The measured XPD at the centre frequency is 28.3 dB. The minimum measured XPD at 26.8 GHz is 25.1 dB when port #1 or #5 is excited. The slight decrease of XPD off the centre frequency is mainly because the phase error introduced by the interconnection is not well compensated at the edge frequencies. The measured results confirm that the cross-polarized radiation in the 2D multibeam antenna array is suppressed by using the differential-feeding technique.

C. Gain

The measured and simulated gain and directivity of the designed dual-polarized multibeam array antenna are illustrated in Fig. 21. When port #1 is excited, the simulated gain increases from 8.4 dBi to 10.8 dBi over the frequency range from 26.8 GHz to 29.2 GHz, while the measured one is in the range of 7.6 dBi – 10.5 dBi. The simulated directivity over the bandwidth is increased from 10.5 dBi to 12.1 dBi. The simulated efficiency at the centre frequency is approximately 55%. The efficiency is mainly degraded by the high loss laminates Rogers 4003C and the fabrication tolerance. In addition, the losses from the connectors are not calibrated. The change of gain and directivity when port #5 is excited has the similar tendency to the results of port #1 under excitation. The slight difference between the measured and simulated gain is mainly caused by the uncertainty of the dielectric loss of the used laminates.

D. Comparison and Discussion

A comparison between our work and the reported 2D multibeam array antennas is carried out in Table. II. The antenna array in [15], has low SLLs, but suffers very narrow bandwidth and low XPDs. The antenna arrays in [19], [20], and [23] have wide bandwidth, but they are only able to operates with a single polarization and their XPDs are lower than 15 dB. Both dual-polarization and wide bandwidth are

achieved in the antenna array reported in [24]. However, this antenna also suffers low XPD, which is only 10 dB when beams scan off the boresight. In comparison, the proposed 2D multibeam antenna array is able to work with dual-polarization while maintaining high XPD when the beams scan to the maximal beam pointing angles. In addition, the designed array antenna can be realized with only two PCB laminates, as the multibeam feeding network for VP is designed with the antenna array aperture on the same laminate layer. Hence, the proposed antenna array also has the advantages of easy fabrication and low cost. Owing to the low profile of the antenna with a thickness of only 0.09λ (λ is the wavelength in the laminate), the developed antenna array is not a wideband antenna. The bandwidth can be improved by increasing the thickness and lowering the permittivity of the laminate as the designs reported in [19], [20], [23] and [24]. As the antenna element separation is designed as $0.7\lambda_0 \times 0.7\lambda_0$, the SLLs are degraded when the beams scan to the maximal pointing angles. This could be mitigated by decreasing the element distance and optimizing the excitation if low SLLs are required in some application scenarios.

V. Conclusion

This paper presents a novel design of mmWave dual-polarized 2D multibeam array antenna. The differentially-driven cavity-backed shorted patch is employed as the antenna element in the design of dual-polarized multibeam array antennas for the first time. The SIW power dividers designed on two laminate layers are used to achieve differential excitations to the antenna elements. Two Butler Matrices placed perpendicularly with each other in different laminates are used to generate four tilted beams with dual-polarization. An antenna prototype working from 26.8 GHz to 29.2 GHz is fabricated and measured. The whole structure is realized by using only two laminates. The measured results and simulated results agree well. When the beams scan to the maximal pointing angles, the measured XPDs in our design are higher than 25 dB within the operation bandwidth. The measured results confirm that the cross-polarization are effectively suppressed in this 2D multibeam antenna array. Compared with the reported works, the proposed dual-polarized 2D multibeam antenna array has the advantages of high XPDs, low profile, ease of fabrication and low cost.

References

[1] W. Hong et al., "Multibeam Antenna Technologies for 5G Wireless Communications," *IEEE Trans. Antennas and Propag.*, vol. 65, no. 12, pp. 6231-6249, Dec. 2017.

[2] F. Foglia Manzillo, R. Nastri, M. Spella, G. Gentile and M. Spirito, "A 60-GHz Passive Broadband Multibeam Antenna System in Fused Silica Technology," *IEEE Antennas Wirel. Propag. Lett.*, vol. 12, pp. 1376-1379, 2013.

[3] Q. Luo, S. Gao, W. Liu and C. Gu, Low-cost smart antennas, John Wiley & Sons, 2019.

[4] F. Foglia Manzillo et al., "A Wide-Angle Scanning Switched-Beam Antenna System in LTCC Technology With High Beam Crossing Levels for V-Band Communications," *IEEE Trans. Antennas and Propag.*, vol. 67, no. 1, pp. 541-553, Jan. 2019.

[5] Q. Yang, Y. Ban, K. Kang, C. Sim and G. Wu, "SIW Multibeam Array for 5G Mobile Devices," *IEEE Access*, vol. 4, pp. 2788-2796, 2016.

[6] Q. Wu, J. Hirokawa, J. Yin, C. Yu, H. Wang and W. Hong, "Millimeter-Wave Multibeam Endfire Dual-Circularly Polarized Antenna Array for 5G Wireless Applications," *IEEE Trans. Antennas and Propag.*, vol. 66, no. 9, pp. 4930-4935, Sept. 2018.

[7] Y. J. Cheng, W. Hong and K. Wu, "Millimeter-Wave Substrate Integrated Waveguide Multibeam Antenna Based on the Parabolic Reflector Principle,"*IEEE Trans. Antennas and Propag.*, vol. 56, no. 9, pp. 3055-3058, Sept. 2008.

[8] A. Artemenko, A. Mozharovskiy, A. Maltsev, R. Maslennikov, A. Sevastyanov and V. Ssorin, "Experimental Characterization of E-Band Two-Dimensional Electronically Beam-Steerable Integrated Lens Antennas," *IEEE Antennas Wirel. Propag. Lett.*, vol. 12, pp. 1188-1191, 2013.

[9] J. Ala-Laurinaho et al., "2-D Beam-Steerable Integrated Lens Antenna System for 5G*E*-Band Access and Backhaul," *IEEE Trans. Microwave Theory Tech.*, vol. 64, no. 7, pp. 2244-2255, July 2016.

[10] R. C. Hansen, *Phased Array Antennas, 2nd ed*. Hoboken, NJ, USA: Wiley, 2009.

[11] B. Pattan, "The Versatile Butler Matrix," *Microwave Journal*, vol. 47, no. 11, pp. 126-138, Nov. 2004.

[12] J. Remez, E. Zeierman and R. Zohar, "Dual-Polarized Tapered Slot-Line Antenna Array Fed by Rotman Lens Air-Filled Ridge-Port Design," *IEEE Antennas Wirel. Propag. Lett.*, vol. 8, pp. 847-851, 2009.

[13] J. Lian, Y. Ban, Q. Yang, B. Fu, Z. Yu and L. Sun, "Planar Millimeter-Wave 2-D Beam-Scanning Multibeam Array Antenna Fed by Compact SIW Beam-Forming Network," *IEEE Trans. Antennas and Propag.*, vol. 66, no. 3, pp. 1299-1310, March 2018.

[14] Y. J. Cheng, W. Hong and K. Wu, "A two-dimensional multibeam array antenna based on substrate integrated waveguide technology," *2008 Asia-Pacific Microwave Conf.*, Macau, 2008, pp. 1-4.

[15] J. Lian, Y. Ban, J. Zhu, J. Guo and Z. Chen, "Planar 2-D Scanning SIW Multibeam Array With Low Sidelobe Level for Millimeter-wave Applications," *IEEE Trans. Antennas and Propag.*, vol. 67, no. 7, pp. 4570-4578, July 2019.

[16] Y. J. Cheng, W. Hong and K. Wu, "Millimeter-Wave Multibeam Antenna Based on Eight-Port Hybrid," *IEEE Microwave Wireless Compon. Lett.*, vol. 19, no. 4, pp. 212-214, April 2009.

[17] W. Yang, Y. Yang, W. Che, C. Fan and Q. Xue, "94-GHz Compact 2-D Multibeam LTCC Antenna Based on Multifolded SIW Beam-Forming Network," *IEEE Trans. Antennas and Propag.*, vol. 65, no. 8, pp. 4328-4333, Aug. 2017.

[18] D. Guan, Y. Zhang, Z. Qian, Y. Li, M. Asaadi and C. Ding, "A Novel 2-D Multibeam Antenna Without Beamforming Network," *IEEE Trans. Antennas and Propag.*, vol. 64, no. 7, pp. 3177-3180, July 2016.

[19] W. F. Moulder, W. Khalil and J. L. Volakis, "60-GHz Two-Dimensionally Scanning Array Employing Wideband Planar Switched Beam Network," *IEEE Antennas Wirel. Propag. Lett.*, vol. 9, pp. 818-821, 2010.

[20] I. M. Mohamed and A. Sebak, "60 GHz 2-D Scanning Multibeam Cavity-Backed Patch Array Fed by Compact SIW Beamforming Network for 5G Applications," *IEEE Trans. Antennas and Propag.*, vol. 67, no. 4, pp. 2320-2331, April 2019.

[21] J. Wang, Y. Li, L. Ge, J. Wang and K. Luk, "A 60 GHz Horizontally Polarized Magnetoelectric Dipole Antenna Array With 2-D Multibeam Endfire Radiation," *IEEE Trans. Antennas and Propag.*, vol. 65, no. 11, pp. 5837-5845, Nov. 2017.

[22] M. M. M. Ali and A. Sebak, "2-D Scanning Magnetoelectric Dipole Antenna Array Fed by RGW Butler Matrix," *IEEE Trans. Antennas and Propag.*, vol. 66, no. 11, pp. 6313-6321, Nov. 2018.

[23] Y. Li, J. Wang and K. Luk, "Millimeter-Wave MultiBeam Aperture-Coupled Magnetoelectric Dipole Array With Planar Substrate Integrated Beamforming Network for 5G Applications," *IEEE Trans. Antennas and Propag.*, vol. 65, no. 12, pp. 6422-6431, Dec. 2017.

[24] Y. Li and K. Luk, "60-GHz Dual-Polarized Two-Dimensional Switch-Beam Wideband Antenna Array of Aperture-Coupled Magneto-Electric Dipoles," *IEEE Trans. Antennas and Propag.*, vol. 64, no. 2, pp. 554-563, Feb. 2016.

[25] S. Liao, P. Wu, K. M. Shum and Q. Xue, "Differentially Fed Planar Aperture Antenna With High Gain and Wide Bandwidth for Millimeter-Wave Application," *IEEE Trans. Antennas and Propag.*, vol. 63, no. 3, pp. 966-977, March 2015.

[26] L. Wen et al., "A Wideband Differentially Driven Dual-Polarized Antenna by Using Integrated Six-Port Power Divider," *IEEE Trans. Antennas and Propag.*, vol. 67, no. 12, pp. 7252-7260, Dec. 2019.

[27] W. R. Eisenstadt, R. Stengel, and B. M. Thompson, *Microwave Differential Circuit Design Using Mixed-Mode S-Parameters*. Boston, MA, USA: Artech House, 2006.

[28] K. Carver and J. Mink, "Microstrip antenna technology," *IEEE Trans. Antennas and Propag.*, vol. 29, no. 1, pp. 2-24, Jan. 1981.

[29] Q. Yang, Y. Ban, J. Lian, Z. Yu and B. Wu, "SIW Butler Matrix with Modified Hybrid Coupler for Slot Antenna Array," *IEEE Access*, vol. 4, pp. 9561-9569, 2016.

[30] D. Kim, J. Hirokawa and M. Ando, "Design of Waveguide Short-Slot Two-Plane Couplers for One-Body 2-D Beam-Switching Butler Matrix Application," *IEEE Trans. Microwave Theory Tech.*, vol. 64, no. 3, pp. 776-784, March 2016.